Protein and lipid dynamics in photosynthetic thylakoid membranes investigated by in-situ solid-state NMR

Azadi Chegeni, F.; Perin, G.; Sai Sankar Gupta, K.B.; Simionato, D.; Morosinotto, T.; Pandit, A.

Biochimica et Biophysica Acta 1857 (2016) 1849–1859

Contents lists available at ScienceDirect

Biochimica et Biophysica Acta

journal homepage: www.elsevier.com/locate/bbabio

Protein and lipid dynamics in photosynthetic thylakoid membranes investigated by *in-situ* solid-state NMR

Fatemeh Azadi Chegeni [a], Giorgio Perin [b], Karthick Babu Sai Sankar Gupta [a], Diana Simionato [b], Tomas Morosinotto [b], Anjali Pandit [a,*]

[a] Leiden Institute of Chemistry, Dept. of Solid State NMR, Leiden University, Einsteinweg 55, 2333CC, Leiden, The Netherlands
[b] PAR-Lab (Padua Algae Research Laboratory), Dept. of Biology, University of Padova, Via Ugo Bassi 58B, 35121 Padova, Italy

ARTICLE INFO

Article history:
Received 7 July 2016
Received in revised form 7 September 2016
Accepted 8 September 2016
Available online 11 September 2016

Keywords:
Photosynthesis
LHCII
Polarization-transfer ssNMR
Zeaxanthin
Biosynthetic isotope labeling
Conformational dynamics

ABSTRACT

Photosynthetic thylakoid membranes contain the protein machinery to convert sunlight in chemical energy and regulate this process in changing environmental conditions via interplay between lipid, protein and xanthophyll molecular constituents. This work addresses the molecular effects of zeaxanthin accumulation in thylakoids, which occurs in native systems under high light conditions through the conversion of the xanthophyll violaxanthin into zeaxanthin via the so called xanthophyll cycle. We applied biosynthetic isotope labeling and ^{13}C solid-state NMR spectroscopy to simultaneously probe the conformational dynamics of protein, lipid and xanthophyll constituents of thylakoids isolated from wild type (*cw15*) and *npq2* mutant of the green alga *Chlamydomonas reinhardtii*, that accumulates zeaxanthin constitutively. Results show differential dynamics of wild type and *npq2* thylakoids. Ordered-phase lipids have reduced mobility and mobile-phase lipids have enlarged dynamics in *npq2* membranes, together spanning a broader dynamical range. The fraction of ordered lipids is much larger than the fraction of mobile lipids, which explains why zeaxanthin appears to cause overall reduction of thylakoid membrane fluidity. In addition to the ordered lipids, also the xanthophylls and a subset of protein sites in *npq2* thylakoids have reduced conformational dynamics. Our work demonstrates the applicability of solid-state NMR spectroscopy for obtaining a microscopic picture of different membrane constituents simultaneously, inside native, heterogeneous membranes.

1. Introduction

Conversion of sunlight into chemical energy takes place inside photosynthetic membranes, where pigment-protein nano-machines carry out a cascade of reactions that evolve in time and space [1]. In order to safely perform the photosynthesis reactions and ensure organism fitness under fluctuating light conditions, constant membrane remodeling takes place. In excess light, feedback deregulation mechanisms induce quenching of sunlight excitations, dissipating the excess light energy as heat and creating a safety valve for the photosynthetic apparatus [2,3]. In plant and algae thylakoids, photosynthesis is regulated through complex interplay between molecular conformational changes, reversible supramolecular interactions and membrane phase transitions [4]. Thylakoids are densely packed with proteins that occupy ~70% of the membrane space and control the membrane phases [5]. Short- and long-term acclimation of thylakoids to light and cold stress involves reorganization of antenna-supercomplexes [4,6–9], conversion of the xanthophyll violaxanthin (Vio) into zeaxanthin (Zea) via the xanthophyll cycle [1] and increase of lipid unsaturation by changing lipid composition [10]. Modulated by low pH, phosphorylation and the xanthophyll cycle, a part of the light-harvesting complex II (LHCII) antenna population disconnects from the Photosystem II (PSII) complexes and self-aggregates to form chlorophyll (Chl)-quenched states, which dissipate excess light [11].

The effects of xanthophyll composition on regulation and photoprotection in thylakoids have been investigated in various studies. Zea is known to play a central role in photoprotection, through its participation in Non-Photochemical Quenching (NPQ) [12] but also by preventing lipid oxidative damage in the membrane [13]. The antioxidant activity of xanthophyll pigments present in membranes was indeed found to be related to their physical-chemical interaction with lipids [14] and their presence was shown to increase the penetration barrier to molecular oxygen [15]. Moreover, several *in vivo* and *in-vitro* studies have reported increased rigidity of Zea-containing membranes [13,16], contributing to their stabilization. The precise role of Zea in NPQ is still under debate. The green microalga *Chlamydomonas reinhardtii*(*Cr.*) *npq2* mutant is defective in Zea epoxidase and has an impaired xanthophyll cycle. In *npq2* lutein and β-carotene are the major carotenoids while it is unable to synthetize antheraxanthin and violaxanthin and accumulates Zea constitutively, under all light conditions. The mutation does not impair the

* Corresponding author.
E-mail address: a.pandit@chem.leidenuniv.nl (A. Pandit).

http://dx.doi.org/10.1016/j.bbabio.2016.09.004
0005-2728/

photoautotrophic growth of *npq2* with respect to the parental strain (*cw15*) in various growing conditions. *Npq2* mutant only showed a decrease in chlorophyll content per cell upon cultivation in high light with a consequent increase in the carotenoid/Chl ratio. *Npq2* mutant showed a decreased quantum yield of PSII (Fv/Fm) [17] but also faster fluorescence quenching upon actinic-light exposure [18,19]. Zea has been suggested to be involved in quenching of excess energy by multiple mechanisms, by activating a quenched state in LHC protein complexes upon binding [20–22] but also at the membrane level, mediating interactions between the complexes [23]. The accumulation of Zea was also demonstrated to protect the polyunsatured lipids, during photooxidative stress, as well as α-tocopherol [13], showing a strong antioxidative effect from Zea independent from its binding to PSII light-harvesting complexes.

In this work, we explored the use of *in-situ* ^{13}C solid-state Nuclear Magnetic Resonance (NMR) on whole thylakoids to gain insight in protein and lipid conformational dynamics and the effect of Zea accumulation. ^{13}C-NMR spectroscopy in conjunction with biosynthetic uniformly ^{13}C isotope labeling provides us with a unique method to simultaneously detect protein, lipid and xanthophyll molecular constituents and measure their molecular dynamics directly. We analyzed *Cr.* thylakoids from wild type (*cw15*) and from *npq2* mutant that, as already mentioned accumulates Zea in the thylakoids. ^{13}C Magic Angle Spinning (MAS) NMR spectra were obtained by direct and cross polarization to separate and quantify rigid and dynamic membrane molecular components. To measure the temperature-dependent dynamical properties, spectra were collected over a temperature range from 0 to 25 °C. In addition, $T_{1\rho}$ relaxation experiments were performed to further analyze protein backbone molecular dynamics. Results show differential dynamics of proteins, lipids and xanthophylls in *cw15* and *npq2* membranes. The *npq2* membranes contain more xanthophylls and ordered-phase lipids with reduced dynamics, as well as mobile-phase lipids with enlarged dynamics, spanning a broader dynamical range. Our study validates the application of ^{13}C solid-state NMR spectroscopy for functional screening of molecular membrane characteristics and demonstrates how Zea accumulation influences the conformational dynamics of protein and lipid constituents, affecting the functionality of heterogeneous thylakoid membranes.

2. Materials and methods

2.1. Chlamydomonas reinhardtii strains and growth conditions

In this work we employed *C. reinhardtii* strains *cw15* and *npq2*. The first is a cell wall-less mutant [24] used as reference, used as a parental strain for the isolation of a mutant depleted in Zea epoxidase (ZE) [25]. Both strains were cultivated in Erlenmeyer flasks with liquid tris-acetate phosphate (TAP) medium, at 100 rpm agitation and 21 °C in a growth chamber. Continuous illumination was provided from cool-white fluorescent lamps under low (< 25 μmoles photons m^{-2} s^{-1}) photosynthetically active radiation (400–700 nm). The TAP medium [26] used to grow labeled cells, was prepared using ^{13}C labeled sodium acetate (Sigma-Aldrich) and ^{15}N labeled ammonium chloride (Sigma-Aldrich). Cultures in labeled medium were set up starting from an optical density at 750 nm (OD_{750}) equal to 0.1 and cells were grown until $OD_{750} = 1$. Three rounds of cultivation in labeled medium were performed to ensure >95% labelling of the cells with ^{13}C and ^{15}N atoms.

2.2. Thylakoid isolation

Cells were harvested by 10 min of centrifugation at 4 °C, at 3500 g and then washed twice in isolation medium A (IMA, 10 mM MES pH 6.5, 2 mM KCl, 5 mM EDTA pH 8, 1 M sorbitol). After centrifugation, cells were resuspended in cold IMA buffer with 0.5% milk powder (commercial food product) and 1 mM PMSF, 1 mM DNP-ε-amino-n-caproic acid and 1 mM benzamidine, and then disrupted at 4 °C using an ultrasonic homogenizer (Sonic Rupter 400 – OMNI International - PBI) for 5 s, with the maximum power. Immediately after rupture, the samples were centrifuged for 15 min at 2500 g at 4 °C to collect unbroken cells on the bottom of the tube. The latter were again resuspended in IMA buffer containing inhibitors and milk powder and treated again with the homogenizer. This step was repeated 3 times to be sure to break all the harvested cells, always collecting the supernatant containing the thylakoids. The latter was centrifuged for 15 min at 2500 g at 4 °C, to eliminate cells debris. The supernatant was then centrifuged for 30 min at 40.000 g at 4 °C to collect the thylakoids. The pellet, containing the thylakoids, was washed twice with isolation medium B (IMB, 10 mM MES pH 6.5, 2 mM KCl, 5 mM EDTA pH 8) and resuspended in T3 buffer (50 mM Hepes-KOH pH 7.5, 5 mM $MgCl_2$, 50% glycerol). Immediately, thylakoids were frozen in liquid nitrogen and stored at −80 °C until use. All steps were performed at 4 °C and in dim light. Thylakoids total pigments were extracted with 80% acetone, and the chlorophyll concentration of the samples was determined spectrophotometrically using specific extinction coefficients [27] and spectral fitting previously described in [28].

2.3. Gel electrophoresis

Coomassie-stained SDS-page was performed using 12.5% Tris-glycine gels as in [29]. Samples were solubilized with a solubilization buffer (4×) containing 30% glycerol, 125 mM Tris pH 6.8, 0.1 M dithiothreitol, 9% SDS and were loaded according to the same amount of membranes determined by Chl assay.

2.4. NMR sample preparation

The thylakoids suspension containing 1.5 mg of Chl (approx. 10 times more in protein content) were pelleted by ultra-centrifugation at 223,000 g for 40 min and transferred into NMR rotor inserts.

2.5. NMR experimental setup

All the NMR spectra were collected with a Bruker Advance-III 750 (17.4 T) solid state NMR spectrometer equipped with a 4 mm CP/MAS trip-probe. Presented 2D ^{13}C-^{13}C proton driven spin diffusion NMR experiments (PDSD) were collected with 256 scans and mixing time of 25 ms at -29 °C. Two-pulse phase modulation (TPPM) decoupling (2 dB) was applied during the t_1 and t_2 periods. Each Polarization Transfer (pt) NMR experiment was performed with 256 scans under SPINAL-64 decoupling (1.8 dB) and the MAS frequency was set to 11.6 kHz. All the ^{13}C spectra were referenced to the carbonyl signal of solid ^{13}C-Tyrosine at 172.2 ppm. CP experiments were performed with the contact time (τ_{CP}) of 2 ms, a recycle delay of 2 s and acquisition time of 20 ms, $\omega_1^C/2\pi$ of 40.3 kHz and ^1H nutation frequency linearly ramped from 80 to 100 kHz. In insensitive nuclei enhancement (INEPT) experiments two delays of 1.25 ms and acquisition time of 80 ms were used. For Direct Polarization (DP) experiments, the delay time was 2 s and acquisition time was set to 43 ms. Presented temperature curves are the averaged results of two independent sets of experiments. As a control, CP and DP experiments were performed on a tri-amino acid ($^{13}C/^{15}N$ N- formyl-Met-Leu-Ple-OH(f-MLF)) using the same pulse sequences. In this case, CP signal intensities were about four times the DP signal intensities, in line with expected enhancement from the ^1H and ^{13}C gyromagnetic ratio.

2.6. $T_{1\rho}$ setting

^{13}C $T_{1\rho}$ experiments were performed at 7 and 25 °C. We applied SPINAL-64 heteronuclear decoupling with 1.5 dB during the relaxation delay. To acquire the spectra after the CP MAS pulse, variable spin-lock pulses from 10 μs to 200 ms were applied. Acquisition time was 11 ms and τ_{CP} was set to 256 μs for all experiments, except where stated otherwise. Relaxation curves were obtained by integrating the

appropriate regions as a function of the relaxation delay in each experiment. The reported rates were determined by fitting the data to stretched- or double-exponentials.

2.7. Temperature calibration

Temperatures were calibrated by analyzing ^{207}Pb NMR chemical shift of lead nitrate $(Pb(NO_3)2)$. The readout temperature was regulated from −2.0 to 20.0 °C within ± 0.1 °C. Effective sample temperature as a function of read out temperature and spinning speed was obtained by using the following formula [30]:

$$T_S = 0.97T_0 + 1.34°C\,exp(\omega_r/7.53\,kHz) - 0.77°C$$

In which T_S is the effective sample temperature (in Kelvin), T_0 read out temperature (Kelvin) and ω_r is referred to MAS rate (kHz).

3. Results

3.1. Isotope labeling and thylakoid extraction

Cr. strains *cw15* (further referred to as WT) and *npq2* were chosen for this work and cultivated according to the following considerations. For detection through solid-state NMR, *Cr.* cells were labeled with carbon (^{13}C) and nitrogen (^{15}N) isotopes growing cells on ^{15}N ammonium chloride and ^{13}C sodium acetate. While ^{15}N labeled ammonium chloride was the only nitrogen source in the medium, *C. reinhardtii* is a photosynthetic organism that is also able to fix CO_2 from the atmosphere to support its photoautotrophic metabolism. However, in mixotrophic conditions in presence of acetate, the latter becomes the prominent carbon source [31]. We exploited this metabolic feature for incorporating ^{13}C providing the carbon source in form of ^{13}C-enriched sodium acetate. Cells were nevertheless exposed to a low light intensity, close to the compensation point, to maintain their photosynthetic metabolism active. Also cells were cultivated in flasks, where CO_2 diffusion from the atmosphere is limited in order to further stimulate acetate assimilation from the medium [32]. Three rounds of cultivation in labeled medium were performed in these conditions with a tenfold dilution at every step. This assured the labeling of a very large majority of the molecules at the end of the cultivation. Thylakoids were then extracted from labeled cells and for analysis, the protein complexes of the photosynthetic apparatus were purified by sucrose gradient centrifugation after mild detergent solubilization (Supplementary Fig. S1 A). The *Cr. npq2* mutant showed a reduced trimeric LHC content with respect to the *cw15* strain, as was already shown in literature [33]. Its inability to synthesize antheraxanthin, violaxanthin and neoxanthin and the constitutive accumulation of Zea even in low light conditions was confirmed by high-pressure liquid chromatography (HPLC) analysis (Supplementary Fig. S1B).

3.2. Characterization by SDS page analysis and by ^{13}C-^{13}C NMR

NMR spectra contain a wealth of structural information because the NMR isotropic chemical shifts are unique fingerprints for each type of atom. However, going from isolated proteins or model lipid membranes to native heterogeneous membranes, spectra become very crowded and individual molecular components are no longer resolved. Thylakoids have the advantage that one class of proteins, the photosynthetic light-harvesting complexes (LHCs), are abundant, reminiscent of recombinantly-expressed proteins in host cell membranes. This is illustrated in Fig. 1, presenting a Coomassie-stained SDS-page analysis of the *Cr.* thylakoid membrane preparations of both *cw15* and *npq2*, loaded with equal volume amounts of membrane material. The light-harvesting complex II (LHCII, indicated with the arrows) appears as the most abundant polypeptides in both strains. The *Cr.* LHCII trimeric complexes are isomers built from polypeptides encoded by 9 genes

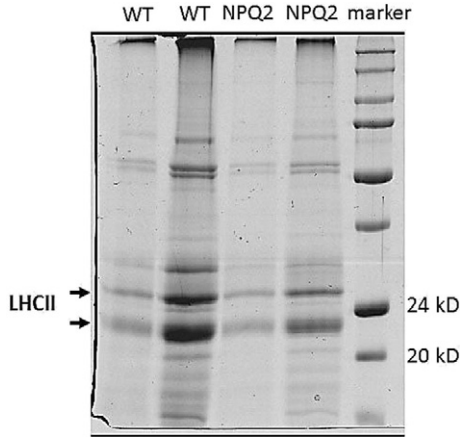

Fig. 1. Coomassie-stained SDS-page of WT and *npq2 Cr.* thylakoids, with 2 μl (lane 1 and 3) or 10 μl (lane 2 and 4) loading of membrane material.

[34,35] with molecular masses between 22 and 26 kDa. Fig. 2 shows a spin-diffusion ^{13}C-^{13}C NMR spectrum (mixing time 25 ms) of the *cw15* and *npq2* thylakoids compared with the one of isolated *Cr.* LHCII. The NMR spectrum of WT thylakoids strongly overlaps with the spectrum of isolated LHCII, indicating that the LHC signals dominate the NMR spectra of thylakoids, consistent with the fact that this is the most abundant protein (Fig. 1 and S1). Nevertheless, the thylakoid spectra are very congested due to the fact that cells were uniformly isotope-labeled and resonances of protein, lipid and pigment constituents are detected simultaneously.

3.3. Polarization transfer solid-state NMR

An elegant way to reduce spectral crowding and improve resolution is by use of NMR ^{1}H-^{13}C polarization-transfer spectral editing. NMR polarization-transfer experiments are selective for molecules with dynamics within a certain frequency window and filter out the NMR signals of all other components. By combining polarization-transfer experiments with different frequency filters, rigid and mobile molecular components are differentiated by their selective enhancement. In addition, the transfer of the magnetization from protons to ^{13}carbons gives rise to signal enhancement owing to the ~4 times enlarged gyromagnetic ratio of ^{1}H compared to ^{13}C. A comparison of polarization-transfer obtained spectra with spectra obtained through direct ^{13}C excitation, which detects signals within a large frequency window, provides an estimation of the rigid and mobile fractions out of the total number of molecular constituents.

To gain insight in protein and lipid molecular dynamics inside thylakoids, a set of one-dimensional solid-state ^{13}C NMR experiments were employed applying ^{1}H-^{13}C polarization-transfer sequences that used cross polarization (CP) [36] or insensitive nuclei enhancement (INEPT) [37], and applying direct ^{13}C polarization (DP) [38]. In DP experiments, the ^{13}C nuclei are directly polarized during the spin-lattice relaxation process and DP detects all molecular constituents. CP and INEPT experiments were applied as frequency filters [39] that are selective for components with slow, resp. Fast molecular dynamics. ^{13}C-detected CP experiments provide NMR spectra of rigid ^{13}C constituents by polarization transfer from ^{1}H nuclei via dipolar couplings. CP signal intensity enhancement depends on the relative gyromagnetic ratios of ^{1}H and ^{13}C, which are $\gamma_H = 267.5$ (10^6 rad S^{-1} T^{-1}) and $\gamma_C = 67.2$ (10^6 rad S^{-1} T^{-1}). The enhancement factor of the CP signal intensity compared to DP is maximal γ_H/γ_C, which is almost a factor of 4. However, the actual enhancement factor depends on molecular motions since the CP technique is based on dipolar ^{1}H-^{13}C couplings, which for very dynamic molecules will average to zero. Mobile constituents, on the other hand, are signal enhanced when the polarization is

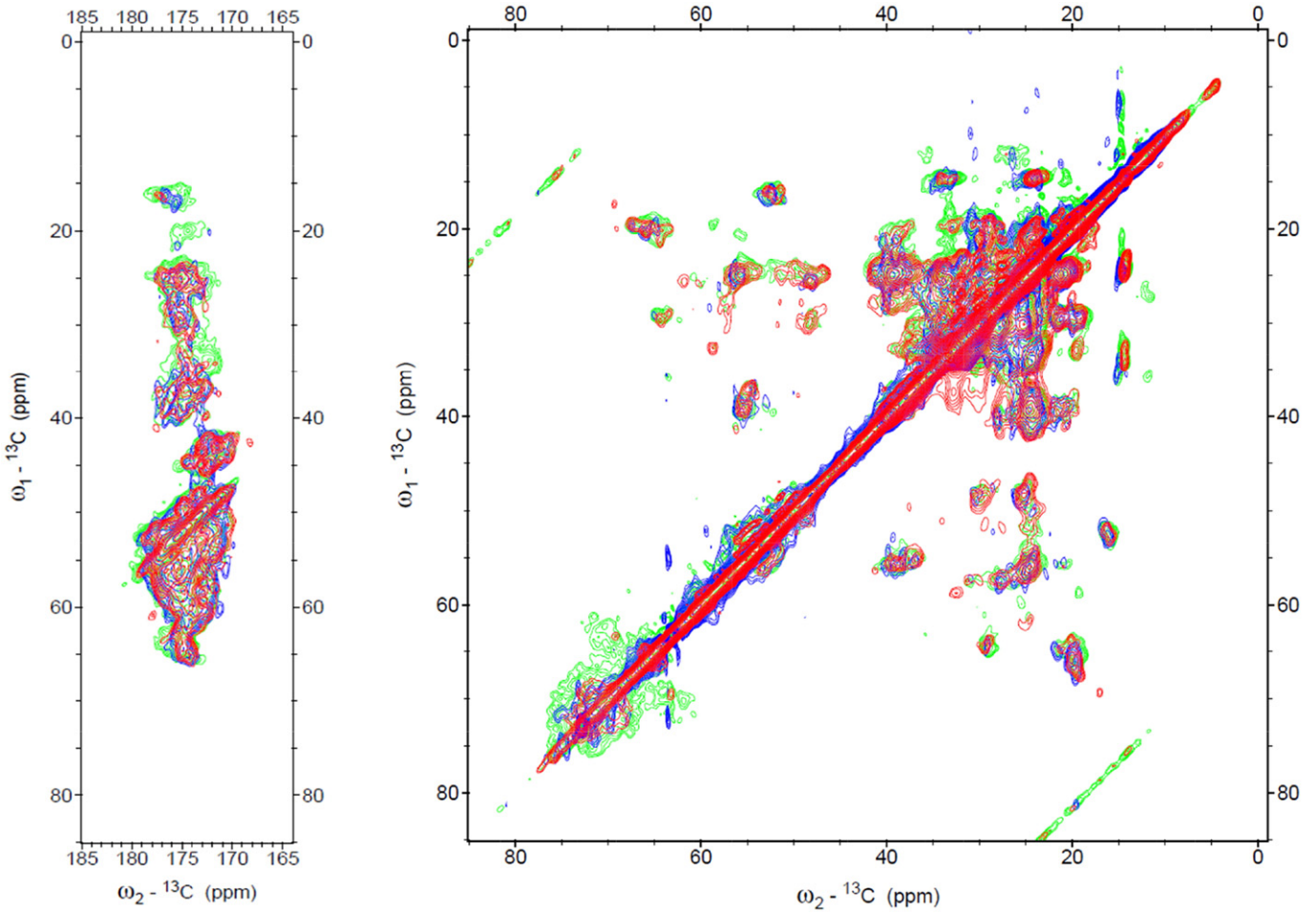

Fig. 2. ^{13}C-^{13}C spectrum of isolated LHCII overlaid on the spectrum of WT (*cw15*) and *npq2* thylakoids. Green; *npq2*, red; LHCII, blue; WT (*cw15*).

transferred via scalar couplings (*J*- couplings), which occur in INEPT. The process of polarization via *J*-couplings is in itself not affected by motions, but scalar coupling occurs in the transverse plane where polarization relaxation (*T2*) depends on motion. Consequently, rigid segments that have fast relaxation times in the transverse plane are not detectable in INEPT [40].

In solid-state NMR spectra of biomembranes, CP-enhanced molecular components typically include lipids with high segmental order in the crystalline phase [41]. Because of their restricted motions, the ^{1}H-^{13}C dipolar couplings are not averaged to zero, making CP efficient, while fast *T2* relaxation excludes their visibility in INEPT spectra. In addition, resonance signals of membrane-embedded proteins, which have restricted conformational dynamics in the millisecond range, are visible in CP-based spectra. INEPT is sensitive for components with fast (sub-nanosecond) dynamics. For bio membranes, these typically include mobile lipids with low segmental order in the fluid gel phase, which have long *T2* relaxation times that makes INEPT efficient, while averaging of the ^{1}H-^{13}C dipolar couplings by bond re-orientation excludes them from CP spectra.

We analyzed thylakoid membrane preparations of *cw15* and *npq2* by ^{13}C MAS NMR using DP, CP and INEPT for mobile spectral editing. In addition, as a comparison the set of experiments was performed on samples of isolated LHCII in β-dodecyl maltoside (β-DM) detergent micelles and of LHCII protein aggregates, obtained by detergent removal, of which preparations have been described in detail in [42]. Fig. 3 illustrates which thylakoid membrane components were signal-enhanced and distinguished performing the CP and INEPT experiments, as described in detail below. In the additional DP experiments, all the in Fig. 3 depicted membrane components are detected. Fig. 4 presents the CP (blue), DP (black) and INEPT (red) ^{13}C MAS-NMR spectral intensities for WT (A) and *npq2* (B) thylakoids and for WT isolated LHCII in detergent micelles (C) and LHCII aggregates (D). The INEPT spectra in Fig. 4 contain NMR signals characteristic for lipids, while CP spectra contain bands typical of the protein backbone and side-chains, as well as peaks typical of lipids. In Fig. 4A and B the lipid galactosyl head-group resonances are obscured by the natural-abundance ^{13}C resonances of glycerol that was present in the thylakoid preparations. The large intensities of the lipid signals in CP (blue spectra) compared to INEPT (red spectra) indicate that the majority of the lipid molecules are in the ordered phase with restrained dynamics, while there is only a small fraction of mobile lipids. The two resonance peaks around 40 ppm are identified as Chl phytol-chain signals that are visible both in CP and INEPT, and a small band between 135 and 140 ppm is identified as the unresolved resonances of the xanthophyll fatty-acyl chains. NMR resonances of the Chl macrocycles are not observed at ambient temperatures and are obscured by protein aromatic signals in 1D spectra. The Chl macrocycle signals can be observed in ^{13}C-^{13}C spectra at cryogenic temperatures [42].

For both the WT and *npq2* membrane preparations, protein signals from the backbone C′ and C_a atoms are more pronounced in DP than in CP, indicating that the proteins have considerable conformational dynamics on micro to millisecond time scales where cross polarization becomes inefficient. As a control, CP and DP experiments were performed on a tri-peptide powder sample using the same pulse sequences (data not shown). In this case, ^{13}C CP signal intensities were roughly four times larger than the directly polarized ^{13}C signal intensities, in line with the maximal expected enhancement of CP based on the ^{1}H and ^{13}C gyromagnetic ratios for a rigid solid. For the WT, the xanthophyll

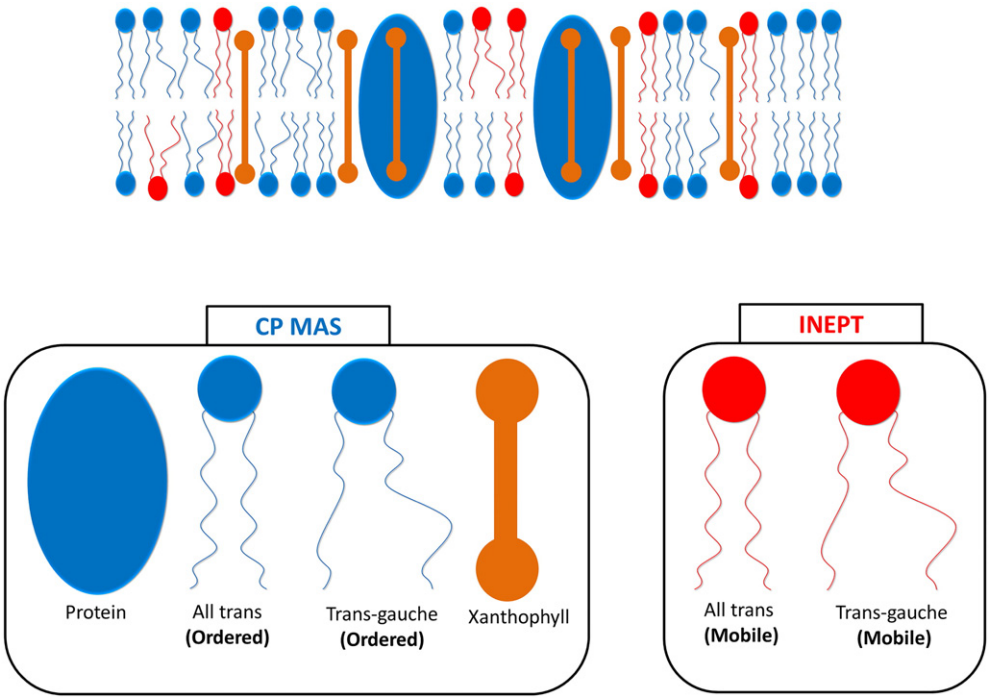

Fig. 3. Illustration of thylakoid constituents that are selectively probed with CP and INEPT experiments, showing the lipids in blue and red, proteins in blue and xanthophylls in orange.

band between 135 and 140 ppm is only observed in DP while for the *npq2* mutant the band appears in CP, indicating that *npq2* mutant contains xanthophylls with reduced fatty-acyl chain dynamics.

No CP signal was detected for LHCII in β-DM micelles (Fig. 4C, blue curve) that undergo fast tumbling in solution, which confirms that the LHCII complexes were fully solubilized, representing a liquid state without protein aggregation. On the contrary, for LHCII aggregates (Fig.4D), strong CP signals are detected. Also here the DP intensities dominate over the CP, as is the case for the thylakoid spectra, indicating that despite their strong aggregation the LHCII complexes possess significant dynamics on sub-millisecond time scales. The ^{13}C NMR spectra of isolated LHCII (Fig. 4C and D) also contain lipid resonances from co-purified lipids. In ^{13}C-^{13}C spectra of LHCII, resonances of the mono-galactosylglycerol (MGDG) and di-galactosylglycerol (DGDG) lipid sugar head groups are resolved [42]. The 2D-resolved resonances confirm that these signals are not natural-abundance ^{13}C resonances of traces of detergent, since the probability of detecting natural-abundance ^{13}carbons in 2D ^{13}C-^{13}C spectra (~0.01%) can be neglected.

3.4. Temperature-dependent dynamics of protein and lipid constituents

To detect molecular dynamics over a physiological temperature range, CP and INEPT spectra were collected between 0 and 25 °C. At high temperatures, a small gradual decrease of the CP intensities is observed, consistent with loss of CP efficiency due to increased molecular dynamics. This is shown in Fig. 5, where the carbonyl C′and C_a integrated peak intensities are plotted against temperature. Simultaneously, INEPT intensities, which detect the dynamic behavior of the mobile-phase lipids, gradually increase with temperature, indicating enlargement of the fraction of mobile lipids. This is illustrated in Fig. 6, presenting the temperature-dependent dynamics of the mobile-phase lipids along their fatty-acyl chains. The end-tails of the mobile lipids are probed via the methyl and (ω-1) CH_2 resonances (6B), and their fatty-acyl chains are detected via their (ω-n) CH_2 resonances (6C) and via the CH resonances (6D). The INEPT fatty-acyl chain intensities of the *npq2* mutant increase more steeply with temperature, indicating enlarged mobility of the mobile lipids in *npq2* membranes at elevated temperatures, compared to the WT.

The dynamics of the ordered lipids with temperature was followed in CP spectra. The lipid peaks here are not fully resolved because they overlap with the broad bands of protein side chains. Fig. 7 shows the CP intensities of the main lipid peak at 30 ppm containing the unresolved (ω-n) CH_2 resonances, and of the small lipid peak at 32 ppm at different temperatures. Lipids can adapt an *all-trans* or *trans*-gauche conformation with different ^{13}C chemical shifts for the acyl chain carbons. The small peak at 32 ppm originates from CH_2 carbons of lipids in the *all-trans* conformation, while the main peak at 30 ppm represents the CH_2 carbons of lipids in *trans*-gauche conformation [43] (see also Figs.4 and 6). The latter lipid conformation is abundant because thylakoids have a high degree of unsaturated lipids. In contrast to other CP signal intensities that decrease at elevated temperatures due to enlarged molecular dynamics, the intensity of the *trans*-gauche lipid peak at 30 ppm increases with temperature. The observed increase is indicative of *all-trans* to *trans*-gauche isomerization. The gain of CP signal due to accumulation of *trans*-gauche lipids is partly compensated by loss of CP efficiency caused by increased lipid mobility. To disentangle the counteracting effects of dynamics and isomerization on the main lipid peak intensity, we compared the 30/32 peak ratios in DP experiments that are insensitive to changes in molecular dynamics. The WT and *npq2* membranes have similar 30/32 ratios at 7 and 25 °C (0.32, resp. 0.42 for WT and 0.32, resp. 0.48 for *npq2*), from which we conclude that the fractions of *trans*-gauche and *all-trans* lipids in the two samples are similar. The differential slopes of the WT (solid lines) and *npq2* (dashed lines) temperature curves in Fig. 7 we therefore ascribe to differential dynamics of the ordered lipids in WT and *npq2*. The ordered lipids in *npq2* apparently are less responsive to temperature changes, with smaller losses of CP efficiencies and have reduced dynamics compared to the WT.

3.5. $T_{1\rho}$ relaxation experiments

In addition to the polarization-transfer experiments, we preformed ^{13}C $T_{1\rho}$ relaxation experiments on the WT and *npq2* thylakoids at 7 and 25 °C. Measurements of spin-lattice longitudinal relaxation in the rotating frame ($T_{1\rho}$) offer investigations of molecular dynamics from microseconds to milliseconds and are sensitive to protein slow

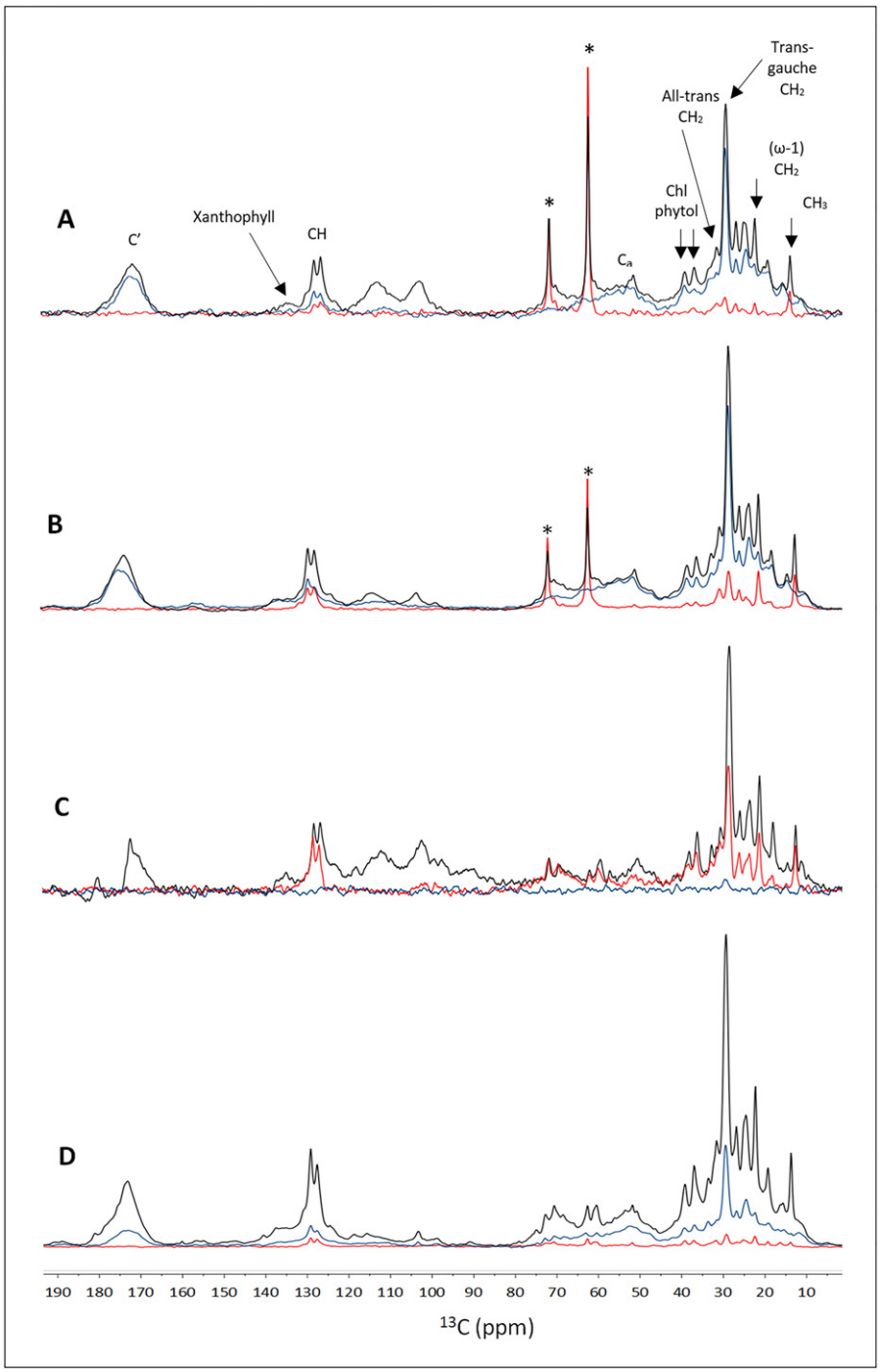

Fig. 4. Overlaid ^{13}C-DP (black), ^{13}C -CP (blue) and ^{13}C-INEPT (red) spectra recorded at 25 °C. A: WT thylakoids; B: *npq2* thylakoids; C: LHCII in detergent micelles; D: LHCII aggregates. *Natural-abundance ^{13}C signals of glycerol.

conformational dynamics. $T_{1\rho}$ describes the decay of magnetization along the RF field B_1, by applying a spin-lock pulse in the rotating frame of reference. Molecular fluctuations with frequencies close to γB_1, i.e. in the range of 10–100 kHz, will induce relaxation of the magnetization along B_1. The ^{13}C $T_{1\rho}$ relaxation rates also depend on the rate of ^{1}H-^{13}C magnetization exchange (K_{HC}) and on the ^{1}H spin-lattice relaxation rate (K_H), as illustrated in the kinetic scheme in Fig. 8. The mixing time during which magnetization is exchanged is set experimentally by the CP contact time, τ_{CP}. We performed ^{13}C $T_{1\rho}$ experiments with $\tau_{CP} = 256$ μs in order to limit proton-driven spin diffusion and inter-carbon magnetization transfer, which both lead to undesired averaging of the $T_{1\rho}$ lifetimes of neighboring carbons. Fig. 9 shows the backbone ^{13}C $T_{1\rho}$ relaxation curves, obtained by integrating the intensities over the backbone C′ band. Instead of a single lifetime, we expect a distribution of lifetimes since the membranes contain a distribution of proteins and each protein contains multiple amino-acid residues with varying structure and dynamics. Therefore C′ $T_{1\rho}$ relaxation curves were fit with stretched exponentials $(e^{-t/T1\rho})^{\beta}$ using a fixed parameter β ($\beta = 0.7$). The C′ $T_{1\rho}$ lifetimes for WT and npq2 are similar at 7 °C, but at 25 °C the C′ $T_{1\rho}$ lifetime is much more shortened for the WT, suggesting enlarged protein dynamics in WT, but not in *npq2* thylakoids. WT $T_{1\rho}$ relaxation curves at 7 °C were also recorded with a longer τ_{CP} of 2 ms. As shown in Table 1, the longer τ_{CP} shortens the C′ $T_{1\rho}$ lifetime from 9.4 to 6.8 ms. C_a $T_{1\rho}$ lifetimes were analyzed by taking the

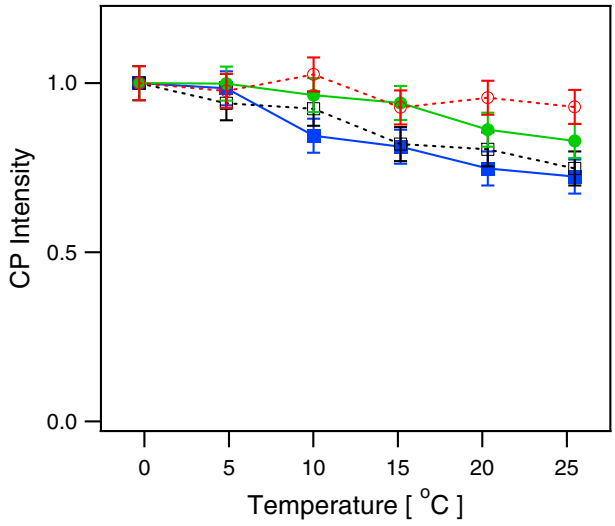

Fig. 5. ^{13}CP-MAS integrated C′ and C_a intensities of WT and *npq2* as function of temperature. Filled blue squares: C′ region WT; open black squares: C′ region npq2; filled green circles: C_a region WT; open red circles: C_a region *npq2*.

integrated intensities over the C_a band (see also Table 1). For some of the C_a data sets, the fit significantly improved if instead of a stretched-exponential a double-exponential fit function was used, which suggests that despite the short τ_{CP} that was applied, the observed C_a relaxation kinetics are partly averaged over the side chain atoms, giving rise to multi-exponential kinetics. Overall, the observed C_a lifetimes were similar at the two temperature conditions and are quite similar for the *npq2* and WT membranes. The C_a $T_{1\rho}$ lifetimes differ significantly from the C′ $T_{1\rho}$ lifetimes, confirming that the C′ relaxation rates contain the characteristics of carbonyl atoms.

The difference between the WT and the *npq2* C′ $T_{1\rho}$ lifetimes seems in apparent contradiction with the carbonyl CP/DP peak intensities in the spectra in Fig. 4, that are very similar for WT and *npq2*. The reason lies in the short τ_{CP} that was used for the $T_{1\rho}$ experiments. Fig. S2 shows the buildup curves for C′ and C_a polarization as function of CP contact times for isolated LHCII. The rise and decay reflect the rates for resp. ^{1}H-^{13}C transfer, building up the carbon magnetization, and for $T_{1\rho}$ spin-lattice relaxation as illustrated in the scheme in Fig. 8. The carbonyl carbons have slow buildup of the polarization because they lack directly attached protons. With $\tau_{CP} = 256$ μs, only a fraction of the C′ carbons are polarized, while with $\tau_{CP} = 2$ ms (used for the experiments presented in Fig. 4) the signal is maximal and all C′ carbons are polarized. As shown in Table 1, the C′ $T_{1\rho}$ lifetime substantially increases with $\tau_{CP} = 256$ μs compared to $\tau_{CP} = 2$ ms. We conclude from these observations that with $\tau_{CP} = 256$ μs only a fraction of C′ carbons is detected, and that these carbons have reduced conformational dynamics. This is consistent with the fact that dynamic carbonyls will have smaller ^{1}H-^{13}C coupling, requiring long contact times for efficient cross polarization. In contrast, the C_a carbons have a fast buildup of the polarization that is already maximal at 256 μs and have fast spin-lattice relaxation, causing loss of signal with longer τ_{CP}. The C_a $T_{1\rho}$ lifetimes thus represent the average of all the C_a carbons. The $T_{1\rho}$ data enables us to identify a fraction of rigid protein carbonyls that only for the WT gain significant dynamics between 7 and 25 °C.

4. Discussion

4.1. Molecular dynamics of LHCII in vivo and of pigment-protein complexes in vitro

Cr. thylakoids are heterogeneous and contain the full photosynthetic apparatus with different protein constituents. Based on the ^{13}C-^{13}C NMR spectra that are dominated by LHCII we can conclude that the observed *in-situ* protein dynamics to large extent represent the properties of LHC proteins. Compared to the lyophilized tri-peptide model used as a control, the proteins inside thylakoids contain considerable dynamics on a microsecond to millisecond time scale, reflected by the relatively low CP/DP intensity ratios. For the LHCII aggregate sample the CP/DP ratios were even lower, implying that in the aggregates the LHCII complexes retain significant mobility that is more comparable with the dynamics of polymers or hydrogels than that of protein crystals. The INEPT spectrum of LHCII aggregates contains a small background signal typical of protein, representing a small fraction of LHCII with high mobility. This suggests that in the aggregate preparations free and aggregated LHCII co-exist in an equilibrium that is strongly shifted towards the aggregated forms. The lipid signals in the LHCII aggregate spectra are much more pronounced in CP than in INEPT, demonstrating that the contained lipids have restrained dynamics and likely are protein associated, and not free lipids from the bulk. The presence of co-purified lipids in purified LHCs is known and LHCII crystal structures of *pea* and *spinach* contain protein-associated lipids [44,45]. No significant CP signal could be detected for LHCII in detergent micelles at ambient temperatures, confirming the absence of protein aggregation. Previous data have shown that CP-based NMR spectra can be obtained of frozen protein-micelle solutions at cryogenic temperatures [42,46,47].

The LHCII Chl macrocycle signals are not detected by CP- neither by INEPT-based ^{13}C-^{13}C spectra at ambient temperatures. Their molecular motions apparently occur on intermediate time scales where both type of experiments are inefficient. The Chl macrocycle NMR resonances of the membrane preparations emerge in NMR spectra at cryogenic temperatures and are weakly visible at 244 K (data not shown). In our previous work, a dynamic transition was revealed between 223 K and 244 K for the Chls in detergent-solubilized LHCII [42] and Chl macrocycle resonances started to disappear from CP-based ^{13}C-^{13}C spectra above 223 K. In line with these NMR observations, quasi-elastic neutron scattering experiments showed a dynamical transition at 244 K for LHCII in detergent micelles [48]. The transition was accompanied with a shift of the Chl *a* absorption maximum that was ascribed to a variety of conformational sub-states of Chl612, based on altered results for a Chl612 mutant. Our previous NMR study also showed that for LHCII aggregates the Chl macrocycle signals are still visible at 244 K, demonstrating that LHCII aggregation reduces Chl conformational dynamics. According to the low-temperature NMR data of thylakoids that will be presented in detail elsewhere, the conformational dynamics of Chls in thylakoids is intermediate between the values for LHCII aggregates and for LHCII detergent micelles. The difference in dynamics suggests that the detergent micelle forms an artificial microenvironment where the LHC pigment-protein complexes are more flexible than in their native states. Liposomal membranes or lipid nano-discs may provide a microenvironment that is closer to their *in-vivo* states [46,49] and it will be of interest to address the dynamics and conformational sub-states of Chls in membrane-reconstituted LHCII.

4.2. Differential dynamics in npq2 and WT membranes: the effects of Zea accumulation

No abrupt changes were detected following CP and INEPT intensities over the range 0-25 °C that would clearly mark a phase transition. Instead, the temperature curves show gradual increase in dynamics of the 'fast' and 'slow' membrane components and of lipid isomerization, consistent with an overall rise of membrane molecular dynamics at elevated temperatures on both fast (ps-ns) and slow (>ms) time scales. In *npq2* membranes, the ordered lipids are less sensitive to temperature changes, whereas the mobile lipids have enlarged dynamics compared to the WT. This effect is the opposite of the reported influence of polar xanthophylls that were shown to act as membrane modulators, increasing membrane fluidity in the ordered phase, while decreasing the fluidity in the liquid crystalline phase, thereby broadening gel-to-fluid phase

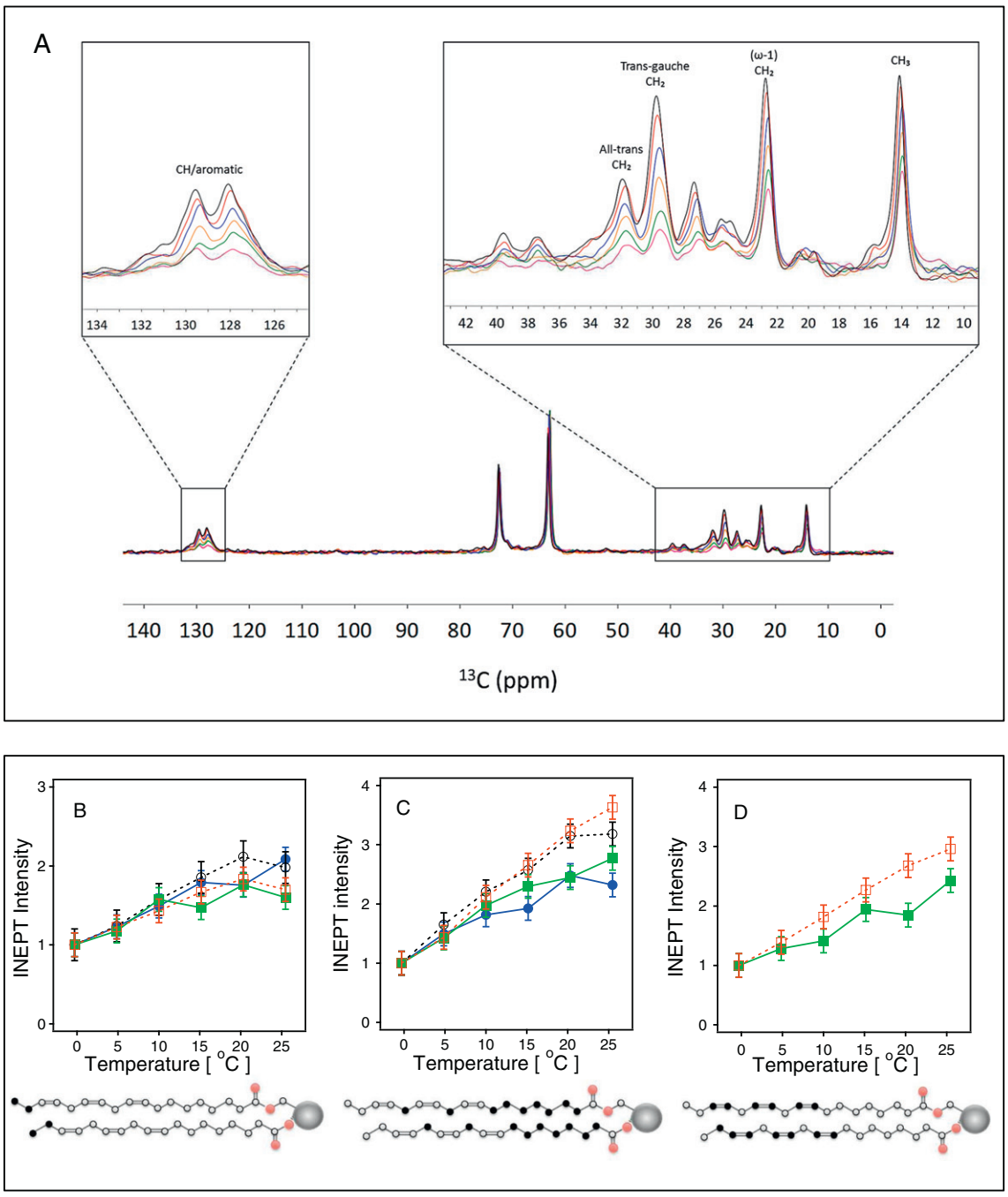

Fig. 6. ^{13}C INEPT intensities of WT and *npq2* membranes as function of temperature. A: Inept spectra of *npq2* recorded at temperatures between 0 and 25 °C. B-D: integrated INEPT spectral regions as function of temperature. The regions correspond to the lipid carbon atoms schematically drawn in the pictures below. A: Filled green squares: CH_3 region, WT; open red squares: CH_3 region *npq2*; filled blue circles: (ω-1) CH_2 region WT; open black circles: (ω-1) CH_2 region *npq2*. B: Filled green squares: *trans*-gauche CH_2 region, WT; open red squares: *trans*-gauche CH_2 region *npq2*; filled blue circles: *all-trans* CH_2 region WT; open black circles: *all-trans* CH_2 region *npq2*. C: Filled green squares: CH/aromatic region, WT; open red squares: CH/aromatic region *npq2*.

transitions [50]. The reverse effect for Zea-accumulating membranes, compared to WT membranes that mainly constitute Vio, could be observed because Zea is a less-polar xanthophyll [20]. Our analysis predicts that Zea-accumulating membranes will have more narrow gel-to-fluid phase transitions, which might be an advantage under stress conditions since this would allow faster switching between the phases.

In both WT and *npq2* thylakoids the fraction of mobile lipids is small compared to the fraction of ordered lipids. The overall membrane fluidity will therefore be dominated by the behavior of the ordered-phase lipids and consequently, is reduced for Zea-containing membranes. The fraction of ordered lipids could represent lipids that are associated with proteins or stabilized in between super complexes, while the mobile lipids represent the bulk lipids that are not in direct protein contact. The restricted dynamics of the majority of the lipids despite their large number of unsaturation suggests that in the tightly packed thylakoids, where greater part of the surface area is protein occupied, most of the lipids are immobilized between the protein complexes.

The slow-dynamic components that are observable via CP could be further separated in rigid and dynamic subsets based on $T_{1\rho}$ relaxation kinetics using short contact times. The $T_{1\rho}$ lifetimes indicate that the *npq2* membranes contain a subset of protein sites with limited conformational dynamics that only modestly respond to temperature changes

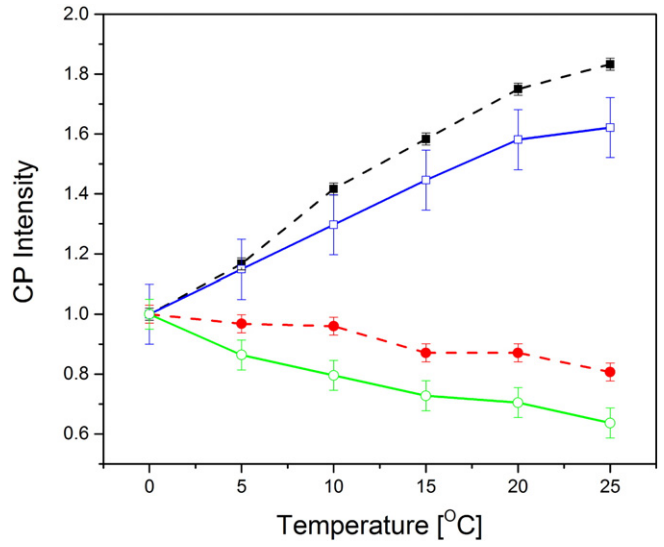

Fig. 7. ^{13}C CP-MAS intensities of WT and *npq2*, illustrating lipid isomerization as a function of temperature. Filled black squares: *trans*-gauche CH_2 region *npq2*; open blue squares: *trans*-gauche CH_2 region WT; Filled red circles: *all-trans* CH_2 region *npq2*; Filled green circles: *all-trans* CH_2 region WT.

between 7 and 25 °C. *Npq2* mutation was shown to not affect photosynthetic apparatus composition, nor photosystems antenna size, even in different light conditions [51]. In the *npq2* membranes, however, LHCII proteins are more prone to monomerization as shown in previous studies in *A. thaliana* [52-55] and confirmed here (Fig. S1 A). Although monomerization could affect the NMR resonances of specific residues and pigments at the monomer-monomer interface in the LHCII trimers, such spectral details are not resolved in the crowded spectra of uniformly-labeled thylakoids presented in Fig. 2. We suspect that monomerization will change the LHCII backbone dynamics. However, rather an increase of flexibility is expected for monomers compared to trimers than the observed reduced protein dynamics in *npq2* thylakoids. In the *npq2* membranes lateral aggregates may have formed in which proteins have restricted conformational dynamics. On the other hand, C′ $T_{1\rho}$ lifetimes of LHCII *in-vitro* aggregates are similar to those of proteins in WT thylakoids. Alternatively, binding of Zea could alter the intrinsic dynamics of LHC proteins at specific sites. Such sites would form a subset of carbonyls that are rigidified in *npq2* thylakoids compared to the WT, conform our $T_{1\rho}$ results. In that respect it is interesting that we also observe reduced conformational dynamics of the xanthophylls in *npq2*. The molecular structure of Zea only differs from Vio, its epoxidized form, at the head group. Due to the de-epoxidized head groups, Zea xanthophylls are more hydrophobic [20], which could change their interactions with the protein direct environments.

Summarizing the results from spectral editing and relaxation experiments, we can conclude that Zea accumulating membranes have (1) more rigid xanthophylls, (2) contain a subset of rigid protein sites that are less sensitive to temperature changes, and (3) contain thylakoid

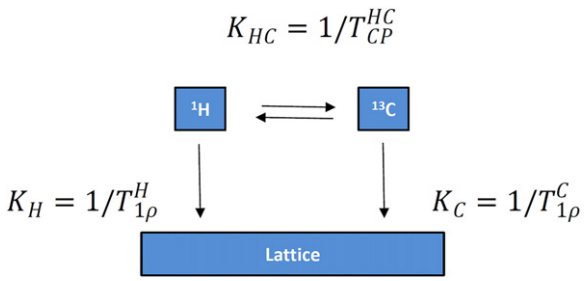

Fig. 8. Kinetic scheme of ^{1}H to ^{13}C polarization transfer and $T_{1\rho}$ spin relaxation.

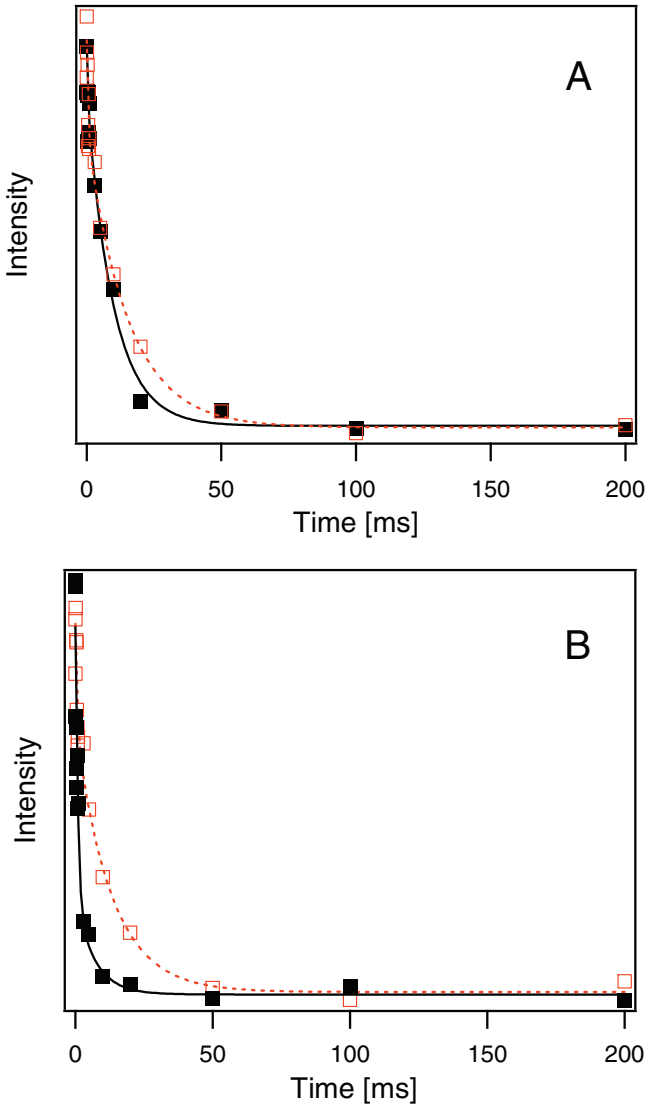

Fig. 9. ^{13}C′ $T_{1\rho}$ relaxation curves of WT and *npq2*. $T_{1\rho}$ relaxation at 7 °C (A) and 25 °C (B) of WT (black filled squares) and *npq2* (red open squares) and stretched-exponential fits (WT, solid black lines; *npq*2, red dashed lines). The fit relaxation lifetimes are 9.4 ms (WT, 7 °C), 10.4 ms (*npq2*, 7 °C), 1.4 ms (WT, 25 °C) and 7.8 ms (*npq2*, 25 °C).

lipids that span a broader dynamical range with reduced fluidity of the large pool of ordered-phase lipids, and enlarged acyl-chain dynamics of the small pool of mobile lipids. Our observation that Zea-rich *npq2* membranes contain xanthophylls, protein and ordered-phase lipid constituents with lower backbone and fatty-acyl chain dynamics is consistent with the detected overall increase in membrane rigidity in Zea-containing membranes as discussed in literature, at least for what concerns *A. thaliana* [52,56]. The co-existence of ordered and mobile lipids suggests that the thylakoids of both WT and *npq2 Cr.* cells contain segregated membrane domains, which may differ in size and composition. Additional electron or atomic-force microscopy would have to be performed to address the effect of Zea accumulation on the supramolecular membrane organization, while additional NMR experiments on Zea-containing LHCII could address the effect of xanthophyll exchange on protein internal molecular dynamics.

4.3. Application of in-situ NMR to photosynthetic membranes

The results of this study demonstrate the ability of biosynthetic isotope labeling and solid-state NMR for assessing protein and lipid molecular dynamics in native, heterogeneous membranes, providing

Table 1
$T_{1\rho}$ lifetimes of the carbonyl and C_a atoms, for WT and *npq2 Cr.* thylakoids and for LHCII aggregates ($LHCII_{agg}$). *Fitting with a double-exponential fit instead of a stretched exponential; value presents the lifetimes of the slow components.

Sample/atom	$T_{1\rho}$ (ms, 7 °C)		$T_{1\rho}$ (ms, 25 °C)	
WT				
C′	9.4 ± 1.5		1.5 ± 0.5	
C_a	1.1 ± 0.3	[2.7 ± 0.9]*	1.0 ± 0.4	[3.1 ± 2.0]*
C′ ($\tau_{CP} = 2$ ms)	6.8 ± 1.1		–	
npq2				
C′	10.4 ± 3.1		7.2 ± 2.2	
C_a	0.7 ± 0.5	[5.0 ± 2.0]*	0.9 ± 0.3	[4.4 ± 1.8]*
$LHCII_{agg}$				
C′	9.5 ± 4.0		1.8 ± 1.3	
C_a	0.9 ± 0.8	[3.6 ± 1.6]*	0.5	[7.9 ± 3.7]*

a microscopic picture on thylakoid organization of *C. reinhardtii* WT and *npq2* mutant strains. The study of Arnold et al. demonstrated that lipid and polysaccharide constituents of micro-algae could be identified by whole-cell NMR using dynamic spectral editing for improving spectral resolution [57]. An interesting idea would be to use polarization-transfer NMR approaches for combined analytical and dynamics screening of photosynthetic cell components. The *in-situ* NMR experiments may also serve as a steppingstone toward structural characterization of LHC pigment-protein complexes in their native environment. While *in-cell* or *in-situ* NMR spectroscopy for structure characterization is very challenging, several studies have been reported, for example solid-state NMR of recombinant-expressed PagL in *E. coli* whole cells and cell envelopes, *in-situ* NMR of the Chl-binding CsmA protein and Dynamic Nuclear Polarization NMR of proteins in native cellular membranes [58,60]. *In-cell* NMR studies that are aimed at structural characterization of a target protein generally rely on genetic manipulation to reduce the background signals of other cellular or membrane components. Recently, a chloroplast biosynthesis induction/repression system was reported to create minimal cells with stripped thylakoids containing LHCII as the only Chl-binding protein [61]. Such system could be explored to create protein selectivity and determine LHCII conformational structure and dynamics *in situ*.

Transparency document

The Transparency document associated with this article can be found, in online version.

Acknowledgements

This work was financially supported by a NWO-CW VIDI grant (granted to AP). Maithili Krishnan is kindly acknowledged for help with the SDS-page analysis.

Appendix A. Supplementary data

Supplementary data to this article can be found online at http://dx.doi.org/10.1016/j.bbabio.2016.09.004.

References

[1] R.E. Blankenship, Molecular mechanisms of photosynthesis, Second edition Wiley/Blackwell, Chichester, West Sussex, 2014.
[2] T.P. Kruger, C. Ilioaia, M.P. Johnson, A.V. Ruban, E. Papagiannakis, P. Horton, R. van Grondelle, Controlled disorder in plant light-harvesting complex II explains its photoprotective role, Biophys. J. 102 (2012) 2669–2676.
[3] J. Cruz, T. Avenson, A. Kanazawa, K. Takizawa, G. Edwards, D. Kramer, Plasticity in light reactions of photosynthesis for energy production and photoprotection, J. Exp. Bot. 56 (2005) 395–406.
[4] H. Kirchhoff, Structural changes of the thylakoid membrane network induced by high light stress in plant chloroplasts, Philos. Trans. R. Soc. Lond. Ser. B Biol. Sci. 369 (2014) 20130225.
[5] H. Kirchhoff, U. Mukherjee, H.J. Galla, H.J. Galla, Molecular Architecture of the Thylakoid Membrane: Lipid Diffusion Space for Plastoquinone, Biochemistry 41 (2002) 4872–4882.
[6] H. Kirchhoff, W. Haase, S. Wegner, R. Danielsson, R. Ackermann, P.A. Albertsson, Low-light-induced formation of semicrystalline photosystem II arrays in higher plant chloroplasts, Biochemistry 46 (2007) 11169–11176.
[7] E. Kouřil, J.B. Wientjes, R. Bultema, E.J. Croce, Boekema, High-light vs. low-light: Effect of light acclimation on photosystem II composition and organization in *Arabidopsis thaliana*, Biochim. Biophys. Acta Bioenerg. 2013 (1827) 411–419.
[8] A.R. Schneider, P.L. Geissler, Coexistence of fluid and crystalline phases of proteins in photosynthetic membranes, Biophys. J. 105 (2013) 1161–1170.
[9] N. Betterle, M. Ballottari, S. Zorzan, S. de Bianchi, S. Cazzaniga, L. Dall'osto, T. Morosinotto, R. Bassi, Light-induced Dissociation of an Antenna Hetero-oligomer Is Needed for Non-photochemical Quenching Induction, J. Biol. Chem. 284 (2009) 15255–15266.
[10] C.W. Mullineaux, H. Kirchhoff, Role of Lipids in the Dynamics of Thylakoid Membranes, 30, 2009 283–294.
[11] A.V. Ruban, C.D.P. Johnson, Duffy, The photoprotective molecular switch in the photosystem II antenna, Biochim. Biophys. Acta Bioenerg. 1817 (2012) 167–181.
[12] E. Erickson, S. Wakao, K.K. Niyogi, Light stress and photoprotection in *Chlamydomonas reinhardtii*, Plant J. 82 (2015) 449–465.
[13] M. Havaux, L. Dall'osto, R. Bassi, Zeaxanthin has enhanced antioxidant capacity with respect to all other xanthophylls in Arabidopsis leaves and functions independent of binding to PSII antennae, Plant Physiol. 145 (2007) 1506–1520.
[14] H.P. McNulty, J. Byun, S.F. Lockwood, R.F. Jacob, R.P. Mason, Differential effects of carotenoids on lipid peroxidation due to membrane interactions: X-ray diffraction analysis, Biochim. Biophys. Acta 1768 (2007) 167–174.
[15] W.K. Subczynski, E. Markowska, J.S. 3, Effect of polar carotenoids on the oxygen diffusion-concentration product in lipid bilayers. An EPR spin label study, Biochim. Biophys. Acta 1068 (1991) 68–72.
[16] P. Jahns, D. Latowski, K. Strzalka, Mechanism and regulation of the violaxanthin cycle: The role of antenna proteins and membrane lipids, Biochim. Biophys. Acta Bioenerg. 1787 (2009) 3–14.
[17] I. Couso, B.F. Cordero, M.A. Vargas, H. Rodriguez, Efficient Heterologous Transformation of *Chlamydomonas reinhardtii* npq2 Mutant with the Zeaxanthin Epoxidase Gene Isolated and Characterized from Chlorella zofingiensis, Mar. Drugs 10 (2012) 1955–1976.
[18] M.J.S.O. Holub, C. Gohlke, Govindjee, G.J. Heiss, R.M. Clegg, Fluorescence lifetime imaging microscopy of *Chlamydomonas reinhardtii*: non-photochemical quenching mutants and the effect of photosynthetic inhibitors on the slow chlorophyll fluorescence transient, J. Microsc. 226 (2006) 90–120.
[19] K.K. Niyogi, A.R. Grossman, O. Björkman, Arabidopsis mutants define a central role for the xanthophyll cycle in the regulation of photosynthetic energy conversion, Plant Cell 10 (1998) 1121–1134.
[20] A.V. Ruban, M.P. Johnson, Xanthophylls as modulators of membrane protein function, Arch. Biochem. Biophys. 504 (2010) 78–85.
[21] N.E. Holt, D. Zigmantas, L. Valkunas, X.-P. Li, K.K. Niyogi, G.R. Fleming, Carotenoid Cation Formation and the Regulation of Photosynthetic Light Harvesting, Science 307 (2005) 433–436.
[22] L. Wilk, M. Grunwald, P.-N. Liao, P.J. Walla, W. Kühlbrandt, Direct interaction of the major light-harvesting complex II and PsbS in nonphotochemical quenching, Proc. Natl. Acad. Sci. 110 (2013) 5452–5456.
[23] P. Xu, L. Tian, M. Kloz, R. Croce, Molecular insights into Zeaxanthin-dependent quenching in higher plants, Sci. Rep. 5 (2015) 13679.
[24] A. CLARKE, G. COULSON, G.J. MORRIS, Relationship between Phospholipid Breakdown and Freezing Injury in a Cell Wall-Less Mutant of Chiamydomonas reinhardii, Plant Physiol. 70 (1982) 97–103.
[25] K.K. Niyogi, O. Bjorkman, A.R. Grossman, Chlamydomonas Xanthophyll Cycle Mutants Identified by Video Imaging of Chlorophyll Fluorescence Quenching, Plant Cell 9 (1997) 1369–1380.
[26] E.H. Harris, The Chlamydomonas Sourcebook. A Comprehensive Guide to Biology and Laboratory Use, Science 246 (1989) (4936–1504).
[27] R.J. Porra, W.A. Thompson, W.A. Kriedemann, Determination of accurate extinction coefficients and simultaneous equations for assaying chlorophylls a and b extracted with four different solvents: verification of the concentration of chlorophyll standards by atomic absorption spectroscopy, Biochim. Biophys. Acta 975 (1989) 384–394.
[28] R. Croce, G. Canino, F. Ros, R. Bassi, Chromophore Organization in the Higher-Plant Photosystem II Antenna Protein CP26, Biochemistry 41 (2002).
[29] U.K. Laemmli, Cleavage of Structural Proteins during the Assembly of the Head of Bacteriophage T4, Nature 227 (1970) 680–685.
[30] X. Guan, R.E. Stark, A general protocol for temperature calibration of MAS NMR probes at arbitrary spinning speeds, Solid State Nucl. Magn. Reson. 38 (2010) 74–76.
[31] R.M. Dent, M.N. Sharifi, A. Malnoe, C. Haglund, R.H. Calderon, S. Wakao, K.K. Niyogi, Large-scale insertional mutagenesis of Chlamydomonas supports phylogenomic functional prediction of photosynthetic genes and analysis of classical acetate-requiring mutants, Plant J. 82 (2015) 337–351.
[32] H. Singh, M.R. Shukla, K.V. Chary, B.J. Rao, Acetate and bicarbonate assimilation and metabolite formation in *Chlamydomonas reinhardtii*: a 13C-NMR study, PLoS One 9 (2014) e106457.
[33] J.E.W. Polle, K.K. Niyogi, A. Melis, Absence of Lutein, Violaxanthin and Neoxanthin Affects the Functional Chlorophyll Antenna Size of Photosystem-II but not that of Photosystem-I in the Green Alga *Chlamydomonas reinhardtii*, Plant Cell Physiol. 42 (2001) 482–491.

[34] J. Minagawa, Y. Takahashi, Structure, function and assembly of Photosystem II and its light-harvesting proteins, Photosynth. Res. 82 (2004) 241–263.
[35] A. Natali, R. Croce, Characterization of the major light-harvesting complexes (LHCBM) of the green alga *Chlamydomonas reinhardtii*, PLoS One 10 (2015) e0119211.
[36] A. Pines, J.S. Waugh, M.G. Gibby, Proton-Enhanced Nuclear Induction Spectroscopy - Method for High-Resolution Nmr of Dilute Spins in Solids, J. Chem. Phys. 56 (1972) 1776.
[37] G.A. Morris, R. Freeman, Enhancement of nuclear magnetic resonance signals by polarization transfer, J. Am. Chem. Soc. 101 (1979) 760–762.
[38] R.N. Purusottam, G. Bodenhausen, P. Tekely, Quantitative one- and two-dimensional 13C spectra of microcrystalline proteins with enhanced intensity, J. Biomol. NMR 57 (2013) 11–19.
[39] A.A. Arnold, B. Genard, F. Zito, R. Tremblay, D.E. Warschawski, I. Marcotte, Identification of lipid and saccharide constituents of whole microalgal cells by (1)(3)C solid-state NMR, Biochim. Biophys. Acta 1848 (2015) 369–377.
[40] P. Diehl, E. Fluck, R. Kosfeld, NMR Basic Principles and Progress / NMR Grundlagen und Fortschritte, Springer-Verlag, Berlin Heidelberg, 1971.
[41] E. Hellstrand, A. Nowacka, D. Topgaard, S. Linse, E. Sparr, Membrane Lipid Co-Aggregation with α-Synuclein Fibrils, PLoS One 8 (2013) e77235.
[42] A. Pandit, M. Reus, T. Morosinotto, R. Bassi, A.R. Holzwarth, H.J.M. de Groot, An NMR comparison of the light-harvesting complex II (LHCII) in active and photoprotective states reveals subtle changes in the chlorophyll a ground-state electronic structures, Biochim. Biophys. Acta Bioenerg. 1827 (2013) 738–744.
[43] R.N. Purusottam, L. Sénicourt, J.-J. Lacapère, P. Tekely, Probing the gel to liquid-crystalline phase transition and relevant conformation changes in liposomes by 13C magic-angle spinning NMR spectroscopy, Biochim. Biophys. Acta Biomembr. 1848 (2015) 3134–3139.
[44] Z. Liu, H. Yan, K. Wang, T. Kuang, J. Zhang, L. Gui, X. An, W. Chang, Crystal structure of spinach major light-harvesting complex at 2.72[thinsp]A resolution, Nature 428 (2004) 287–292.
[45] J. Standfuss, A.C. Terwisscha van Scheltinga, M. Lamborghini, W. Kühlbrandt, Mechanisms of photoprotection and nonphotochemical quenching in pea light-harvesting complex at 2.5 Å resolution, EMBO J. 24 (2005) 919–928.
[46] A. Pandit, T. Morosinotto, M. Reus, A.R. Holzwarth, R. Bassi, H.J.M. de Groot, First solid-state NMR analysis of uniformly 13C-enriched major light-harvesting complexes from *Chlamydomonas reinhardtii* and identification of protein and cofactor spin clusters, Biochim. Biophys. Acta Bioenerg. 1807 (2011) 437–443.
[47] A. Pandit, F. Buda, A.J. van Gammeren, S. Ganapathy, H.J.M. de Groot, Selective Chemical Shift Assignment of Bacteriochlorophyll a in Uniformly [13C — 15 N]-Labeled Light-Harvesting 1 Complexes by Solid-State NMR in Ultrahigh Magnetic Field, J. Phys. Chem. B 114 (2010) 6207–6215.
[48] K. Vrandecic, M. Rätsep, L. Wilk, L. Rusevich, M. Golub, M. Reppert, K.-D. Irrgang, W. Kühlbrandt, J. Pieper, Protein Dynamics Tunes Excited State Positions in Light-Harvesting Complex II, J. Phys. Chem. B 119 (2015) 3920–3930.
[49] P. Akhtar, K. Pawlak, L. Kovacs, A. Bota, M. Dorogi, L. Kovács, A. Bóta, T. Kiss, G. Garab, P. Lambrev, Pigment Interactions in Light-harvesting Complex II in Different Molecular Environments, J. Biol. Chem. 290 (2015) 4877–4886.
[50] W.I. Gruszecki, K. Strzałka, Carotenoids as modulators of lipid membrane physical properties, Biochim. Biophys. Acta (BBA) - Mol. Basis Dis. 1740 (2005) 108–115.
[51] L. Kalituho, J. Rech, P. Jahns, The roles of specific xanthophylls in light utilization, Planta 225 (2007) 423–439.
[52] F. Tardy, M. Havaux, Thylakoid membrane fluidity and thermostability during the operation of the xanthophyll cycle in higher-plant chloroplasts, Biochim. Biophys. Acta 1330 (1997) 179–193.
[53] H. Lokstein, L. Tian, J.E.W. Polle, D.D. Penna, Xanthophyll biosynthetic mutants of *Arabidopsis thaliana*: altered nonphotochemical quenching of chlorophyll fluorescence is due to changes in Photosystem II antenna size and stability, Biochim. Biophys. Acta 1553 (2002) 309–319.
[54] M. Havaux, L. Dall'Osto, S. Cuine, G. Giuliano, R. Bassi, The effect of zeaxanthin as the only xanthophyll on the structure and function of the photosynthetic apparatus in *Arabidopsis thaliana*, J. Biol. Chem. 279 (2004) 13878–13888.
[55] L. Dall'Osto, S. Caffarri, R. Bassi, A mechanism of nonphotochemical energy dissipation, independent from PsbS, revealed by a conformational change in the antenna protein CP26, Plant Cell 17 (2005) 1217–1232.
[56] M. Havaux, Carotenoids as membrane stabilizers in chloroplasts, Trends Plant Sci. 3 (1998) 147–151.
[57] A.A. Arnold, B. Genard, F. Zito, R. Tremblay, D.E. Warschawski, I. Marcotte, Identification of lipid and saccharide constituents of whole microalgal cells by 13C solid-state NMR, Biochim. Biophys. Acta Biomembr. 1848 (2015) 369–377.
[58] M. Renault, R. Tommassen-van Boxtel, M.P. Bos, J.A. Post, J. Tommassen, M. Baldus, Cellular solid-state nuclear magnetic resonance spectroscopy, Proc. Natl. Acad. Sci. 109 (2012) 4863–4868.
[59] N. Kulminskaya, M. Miller, M. Pedersen, M. Bjerring, J. Underhaug, M. Pedersen, M. Bjerring, J. Underhaug, N. Nielsen, N.-U. Frigaard, J. Nielsen, In Situ Solid-State NMR Spectroscopy of Protein in Heterogeneous Membranes: The Baseplate Antenna Complex of Chlorobaculum tepidum, Angew. Chem. Int. Ed. 51 (2012) 6891–6895.
[60] K. Yamamoto, M. Caporini, S.-C. Im, L. Waskell, A. Ramamoorthy, Cellular solid-state NMR investigation of a membrane protein using dynamic nuclear polarization, Biochim. Biophys. Acta Biomembr. 1848 (2015) 342–349.
[61] E. Dinc, S. Ramundo, R. Croce, J.D. Rochaix, Repressible chloroplast gene expression in Chlamydomonas: A new tool for the study of the photosynthetic apparatus, Biochim. Biophys. Acta Bioenerg. 1837 (2014) 1548–1552.